

## Turbulent Heat Fluxes during an Extreme Lake-Effect Snow Event<sup>✉</sup>

AYUMI FUJISAKI-MANOME,<sup>a,b</sup> LINDSAY E. FITZPATRICK,<sup>a</sup> ANDREW D. GRONEWOLD,<sup>c,d</sup>  
ERIC J. ANDERSON,<sup>d</sup> BRENT M. LOFGREN,<sup>d</sup> CHRISTOPHER SPENCE,<sup>e</sup> JIQUAN CHEN,<sup>f</sup>  
CHANGLIANG SHAO,<sup>g</sup> DAVID M. WRIGHT,<sup>b</sup> AND CHULIANG XIAO<sup>a</sup>

<sup>a</sup> Cooperative Institute for Great Lakes Research, University of Michigan, Ann Arbor, Michigan

<sup>b</sup> Department of Climate and Space Sciences and Engineering, University of Michigan, Ann Arbor, Michigan

<sup>c</sup> Department of Civil and Environmental Engineering, University of Michigan, Ann Arbor, Michigan

<sup>d</sup> NOAA/Great Lakes Environmental Research Laboratory, Ann Arbor, Michigan

<sup>e</sup> Environment and Climate Change Canada, Saskatoon, Saskatchewan, Canada

<sup>f</sup> Department of Geography, Environment, and Spatial Sciences, Michigan State University, East Lansing, Michigan

<sup>g</sup> Institute of Agricultural Resources and Regional Planning, Chinese Academy of Agricultural Sciences, Beijing, China

(Manuscript received 7 April 2017, in final form 21 September 2017)

### ABSTRACT

Proper modeling of the turbulent heat fluxes over lakes is critical for accurate predictions of lake-effect snowfall (LES). However, model evaluation of such a process has not been possible because of the lack of direct flux measurements over lakes. The authors conducted the first-ever comparison of the turbulent latent and sensible heat fluxes between state-of-the-art numerical models and direct flux measurements over Lake Erie, focusing on a record LES event in southwest New York in November 2014. The model suite consisted of numerical models that were operationally and experimentally used to provide nowcasts and forecasts of weather and lake conditions. The models captured the rise of the observed turbulent heat fluxes, while the peak values varied significantly. This variation resulted in an increased spread of simulated lake temperature and cumulative evaporation as the representation of the model uncertainty. The water budget analysis of the atmospheric model results showed that the majority of the moisture during this event came from lake evaporation rather than a larger synoptic system. The unstructured-grid Finite-Volume Community Ocean Model (FVCOM) simulations, especially those using the Coupled Ocean–Atmosphere Response Experiment (COARE)–Met Flux algorithm, presented better agreement with the observed fluxes likely due to the model’s capability in representing the detailed spatial patterns of the turbulent heat fluxes and the COARE algorithm’s more realistic treatment of the surface boundary layer than those in the other models.

### 1. Introduction

Communities around the world are becoming increasingly dependent on numerical geophysical model-based forecasts in order to prepare for and respond to hazardous mesoscale weather and hydrologic events (Weisman et al. 2015). As the spatiotemporal resolution of the models increases, it is important to understand how model simulations compare to measurements at corresponding model grid points and how alternative models for meteorological boundary conditions (i.e.,

forcing) propagate into variability within a forecast ensemble. This understanding is particularly important for improving lake-effect snow (LES) forecasts, partly because there is often sparse monitoring data for verifying simulations of the turbulent heat fluxes from the lake surface, and partly because of the severe impacts LES events can have on society.

LES is a common mesoscale event of convective precipitation downwind of midlatitude lakes. It is a manifestation of the development and evolution of a convective internal boundary layer, that is, induced when cold air flows over a relatively warm lake surface (Cordeira and Laird 2008; Notaro et al. 2013; Vavrus et al. 2013). LES events can be particularly pronounced downwind of the Laurentian Great Lakes, where the heat and moisture from the massive lake surfaces can propagate into rapid, life-threatening

<sup>✉</sup> Supplemental information related to this paper is available at the Journals Online website: <https://doi.org/10.1175/JHM-D-17-0062.s1>.

Corresponding author: Ayumi Fujisaki-Manome, [ayumif@umich.edu](mailto:ayumif@umich.edu)

storms. Accurate predictions of LES are challenging for operational weather models. Past studies on LES have focused on different physical aspects, including snowband formation (Hjelmfelt 1990; Niziol et al. 1995) and upwind static stability (Kristovich and Laird 1998). The knowledge gained from these studies has led to the ability to anticipate LES occurrences at operational forecast offices. However, detailed predictions of intensity, timing, and location have to rely on numerical model predictions. Increasing computational capacity has enabled higher spatial resolutions in numerical modeling studies. Several numerical modeling studies on LES had horizontal grid sizes of 2–5 km (Wright et al. 2013; Reeves and Dawson 2013; Conrick et al. 2015), which resolve some snowbands. These numerical modeling studies showed that LES predictions are significantly influenced by their choice of finescale parameterizations, including those of microphysics (Reeves and Dawson 2013) and planetary and surface boundary layers (Conrick et al. 2015). However, one problem lies in the difficulty in determining which parameterization is superior to the others, mainly because of insufficient observations for the direct evaluation of each process.

The surface boundary layer parameterization, also known as surface turbulent heat flux modeling, is a critical factor in accurate LES predictions, as implied by the sensitivity study by Conrick et al. (2015). This makes intuitive sense: absorption of heat and moisture by an air parcel moving over a lake, expressed as turbulent heat fluxes, can be directly tied to snowband formation. We hypothesized that any inadequacies in existing simulations of snowfall from operational weather models might be due to inaccuracies in simulated overlake turbulent heat fluxes. To date, we know of no comparison between modeled and observed turbulent heat fluxes on Lake Erie that might provide insight into numerical model performance simulating lake-effect snow events.

The recent introduction of eddy covariance–based measurements across the Great Lakes provides an opportunity to validate model-simulated fluxes, including those during LES events. These systems calculate the covariance of vertical air motion, surface air temperature, and humidity due to eddy motions in the turbulent planetary boundary layer to derive latent and sensible heat fluxes. This type of measurement was initiated in 2008 over Lake Superior, the largest of the Great Lakes, through the establishment of the Great Lakes Evaporation Network (GLEN), which has since evolved into five eddy covariance stations across the Great Lakes (Blanken et al. 2011; Lenters et al. 2013; Spence et al. 2011, 2013). The Long Point lighthouse

has been a base for eddy covariance measurements on Lake Erie since 2012 (Fig. 1). Another effort to make direct eddy covariance measurements over the Great Lakes was initiated by the Lake Erie Center Sensor Network (LECSN), which includes two eddy covariance stations on western Lake Erie with a relatively stronger focus on the exchange of carbon, water, and key ancillary ecosystem parameters (Shao et al. 2015; Ouyang et al. 2017). It is a crucial step for improved LES predictions to evaluate state-of-the-art numerical models in simulating the turbulent heat fluxes during an LES event by utilizing the direct flux measurements. This will lead to verification and future improvement of the surface boundary layer modeling in numerical models.

While evaluation of modeled turbulent heat fluxes during an LES event is a primary interest in this study, another interest is to assess how much LES can be attributed to evaporation from Lake Erie. There have been studies to understand the impacts of lake surface conditions on LES events, including ice cover on Lake Erie (Cordeira and Laird 2008; Wright et al. 2013; Vavrus et al. 2013) and the evolution of the convective boundary layer over Lake Michigan (Kristovich et al. 2003). However, no previous study has evaluated the extent to which lake evaporation contributes to LES relative to moisture from a larger synoptic system; in the case of this study, this includes Lakes Michigan and Superior as well as regions farther upwind. A recent field campaign involving the Ontario Winter Lake-effect Systems (OWLeS; Kristovich et al. 2016) had a relatively wide range of scientific focus areas, including the surface fluxes from lakes. While their observational data may provide some answers to these questions in the future, such efforts appear to be still in the beginning stage.

This study examined two critical questions: 1) How do operational numerical forecast models perform in simulating the sensible and latent heat fluxes during an extreme LES event in comparison with direct flux measurements? and 2) How much of the precipitation during an LES event can be attributed to evaporation from Lake Erie?

By addressing these questions, we aim to verify the potential for numerical models to simulate turbulent heat fluxes and understand how they relate to snowfall during an LES event. As a natural extension of the analysis, we evaluated the snow water equivalent (SWE), simulated by atmospheric models with a focus on the downwind regions of Lake Erie. The ultimate goal was to provide a recommendation on alternative surface boundary conditions of overlake heat fluxes for improved forecasting of similar dangerous events.

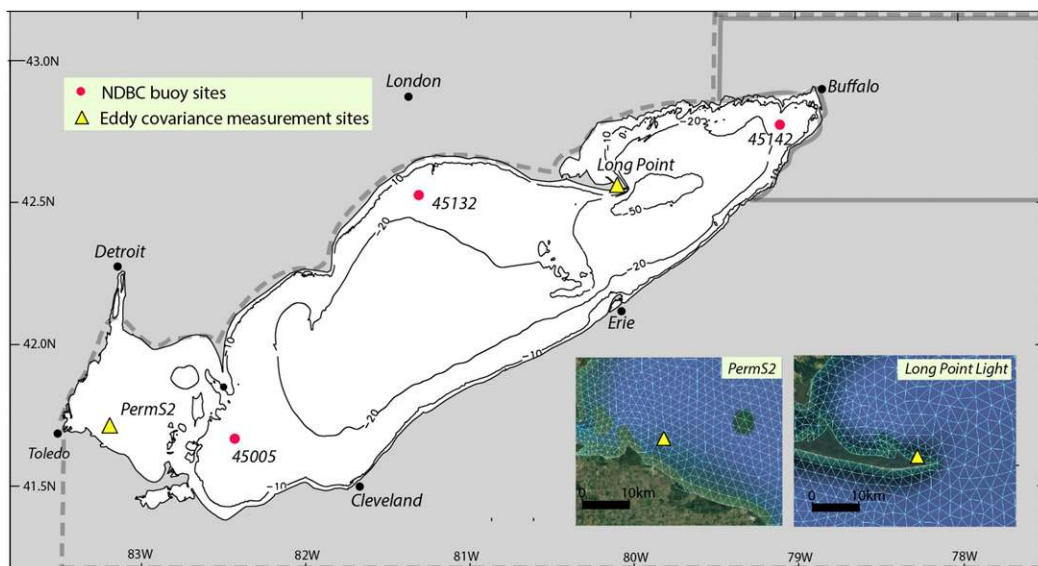


FIG. 1. Map of Lake Erie including the locations of two eddy covariance stations (yellow triangles) at the Toledo water crib intake (Perms2) and the Long Point Lighthouse (Long Point) as well as three NDBC buoy sites (red dots). The overwater domain is used for the hydrodynamic simulations with FVCOM. The bathymetry contours of 10, 20, and 50 m are shown. Zoomed regions around the PermS2 and Long Point stations from Google Earth are shown in the lower right, overlaid with unstructured FVCOM grid. The main and subdomains surrounded by dashed and solid gray lines, respectively, are the regions used for comparison of the SWE. The two domains share the northern and eastern boundaries.

## 2. Methods

### a. LES case study

We focused on a record LES event in the Buffalo, New York, metropolitan area, which was triggered by an extreme North American cold wave in November 2014. The regional snowfall severely impacted the local community: there were at least 13 fatalities, thousands of stranded motorists, power outages, and food and supply shortages (Nason 2014). The LES event included two storms. The first storm started on the evening of 17 November 2014 at 1800 EST (2300 UTC), during which time  $\sim 1$  m of snow fell within the first 12 h, and an additional 1.5 m fell over the remaining 36 h to the east of Buffalo (National Weather Service 2014a). The second storm arrived on the evening of 19 November 2014 at 2300 EST (0400 UTC 20 November) with an additional 1 m of snow (National Weather Service 2014b).

We focus on this event because operational forecast models are in critical need of being evaluated in terms of such a record-setting event, especially when new observations allow verification of previously unverified model variables (i.e., turbulent heat fluxes over a lake).

### b. The models

We assembled a suite of numerical models that are used operationally and experimentally to forecast and nowcast

lake and weather conditions. These models included the Climate Forecast System version 2 (CFSv2; Saha et al. 2014, 2010), the North American Mesoscale Forecast System (NAM; Rogers et al. 2009), the unstructured-grid Finite-Volume Community Ocean Model (FVCOM; Chen et al. 2013, 2006), and the Large Lake Thermodynamic Model (LLTM; Croley 1989a,b; Croley and Assel 2002; Hunter et al. 2015). For the Great Lakes region, NAM and CFSv2 can be mainly considered as atmospheric models, and they are not meant to resolve detailed hydrodynamics of the lakes. On the other hand, FVCOM and LLTM mainly focus on lake physics but do not simulate atmospheric processes. An important process common to all the models is turbulent heat change at the air-lake interface, which we evaluate in this paper. FVCOM was largely used in this study because it was recently transferred into an operational environment and could serve as a new lake physics component of NAM, CFSv2, and possibly other models.

First, these models were verified in terms of meteorological variables that served as surface boundary conditions for the models, simulations of lake water temperature, and single-point latent and sensible heat fluxes. Second, the modeled latent and sensible heat fluxes were intercompared based on the spatial patterns, lakewide means, and cumulative evaporation during the LES event. Third, a water budget analysis

TABLE 1. Twelve model runs used in the study.

ID	Name	Core physical model	Flux algorithm	Boundary conditions	Lake physics	Horizontal resolution/data interval	Other
1	NAM	WRF Model	<a href="#">Łobocki (1993)</a>	GFS, RTG_SST_HR (water surface temperature initial conditions)	Treated as ocean cells in MOM	12 km/6 hourly	<a href="#">Rogers et al. (2009)</a> , <a href="#">Janjić and Gall (2012)</a> ; microphysics: <a href="#">Aligo et al. (2017)</a>
2	CFSv2	GSM and MOM	<a href="#">Long (1986, 1990)</a>	—	—	0.2° (~17 km)/hourly	<a href="#">Saha et al. (2010, 2014)</a> ; microphysics: <a href="#">Zhao and Carr (1997)</a> , <a href="#">Moorthi et al. (2016)</a>
3	FVCOM	The unstructured-grid Finite-Volume Community Ocean Model	COARE ( <a href="#">Fairall et al. 1996a,b</a> )	HRRR	3D hydrodynamic model	200 m (nearshore)–3 km (offshore)/hourly	
4				Interp			
5				CFSv2			
6			<a href="#">LS87 (Liu and Schwab 1987)</a>	HRRR			
7				Interp			
8				CFSv2			
9			<a href="#">J99 (Jordan et al. 1999; Hunke et al. 2015)</a>	HRRR			
10				Interp			
11				CFSv2			
12	LLTM	Large Lake Thermodynamic Model	<a href="#">Croley (1989b)</a>	Integrated Surface Hourly Database	1D thermodynamic model based on a lumped parameter	Lake average/daily	<a href="#">Hunter et al. (2015)</a> ; <a href="#">Croley (1989a,b)</a>

was conducted using the NAM and CFSv2 results. Finally, SWE values, integrated over control areas downwind of Lake Erie from NAM and CFSv2, were compared with observational data. The SWE evaluation was a natural extension of our analyses but was not intended to ascribe all differences between simulation results and observational analyses to modeling of turbulent heat fluxes.

Outputs from 12 different model runs were compared and verified in simulating turbulent heat fluxes (Table 1). NAM and CFSv2 (ID numbers 1 and 2 in Table 1) represent state-of-the-art operational weather forecasting systems at the NOAA Environmental Modeling Center at the National Centers for Environmental Prediction (NCEP) with real-time data assimilation systems to incorporate all available observations, including those of surface meteorology from buoys. NAM uses the Weather and Research Forecasting (WRF) Model ([Skamarock et al. 2008](#)) for its physical model; it has a spatial resolution of 12 km ([Rogers et al. 2009](#)) and provides national weather forecasts of up to 84 h. The water surface temperature is initialized with NOAA's real-time global sea surface temperature analysis (RTG\_SST\_HR; [http://polar.ncep.noaa.gov/sst/rtg\\_high\\_res/](http://polar.ncep.noaa.gov/sst/rtg_high_res/)), and lateral boundary conditions are provided by NCEP's Global Forecast

System (GFS) forecasts, which consist of an atmospheric model based on the Global Spectral Model (GSM) and an ice–ocean model based on the Modular Ocean Model version 4 (MOM). CFSv2 is a global, fully-coupled atmosphere–ocean–land model ([Saha et al. 2014, 2010](#)) that provides operational seasonal global climate forecasts. CFSv2 has many overlaps with GFS (e.g., it uses GSM and MOM) but has a stronger focus on seasonal or longer ranges. Hourly forecasts are provided with a horizontal resolution of 0.2°. In NAM and CFSv2, the Great Lakes are treated as ocean cells, and turbulent heat fluxes at the air–lake interface are calculated with bulk formulae where transfer coefficients are estimated by similarity theory–based approaches. Both models used 6-h forecasts initiated from operational analyses.

Next we describe two models, FVCOM (ID numbers 3–11 in Table 1) and LLTM (ID number 12 in Table 1), that focus on lake physics. Unlike NAM and CFSv2, these models do not simulate atmospheric variables such as downstream effects on snowfall and SWE, but they still simulate the turbulent heat fluxes at the lake surface. FVCOM is a three-dimensional, unstructured-grid hydrodynamic model ([Chen et al. 2006, 2013](#)). It is the physical base of the next-generation NOAA Great Lakes Operational Forecast System (GLOFS) that provides real-time nowcasts and forecasts of lake

conditions. Nine FVCOM simulations were conducted using three sources of meteorological forcings and three internal surface flux calculation algorithms to evaluate the range of the modeled sensible and latent heat fluxes ( $H$  and  $\lambda E$ , respectively) as a function of the model setup, as well as the resulting surface temperature and heat content of the lake. Acronyms in Table 1 categorized under flux algorithms and boundary conditions of FVCOM are described later in section 2c.

LLTM (Croley 1989a,b; Croley and Assel 2002; Hunter et al. 2015) is a lumped-parameter model of evaporation and thermodynamic fluxes for the Great Lakes. LLTM was developed for hydrological research and forecasting, and it has provided long-term lake evaporation estimates going back to the 1950s and forecasts as a component of net basin supplies. The model is forced by meteorology conditions based on overland observations from the Integrated Surface Hourly Database at the National Centers for Environmental Information (Smith et al. 2011). In LLTM, the overland meteorological observations are corrected to overlake values using regression equations (Croley 1989a,b) that include the impacts of atmospheric stability. Note that this correction method is hardwired to LLTM along with the Integrated Surface Hourly Database and therefore does not have the capability to test sensitivity to different forcing datasets like FVCOM does. LLTM runs on a one-dimensional basis. Each model variable in LLTM represents a lakewide average. The model is proven to reproduce annual-mean heat content and lake surface temperature in Lake Michigan in reasonable agreement with the interannual records of satellite and thermistor observations (Gronewold et al. 2015). LLTM is a part of the Great Lakes Advanced Hydrologic Prediction System (AHPS), which is used by the U.S. Army Corps of Engineers (USACE), Environment and Climate Change Canada, New York Power Authority (NYPA), and Ontario Power Generation (OPG) to provide operational water level forecasts.

We compared and verified the meteorological variables (i.e., surface air temperature, relative humidity, wind speed, and wind direction) from NAM, CFSv2, and the forcing datasets to those of FVCOM and LLTM, simulated  $\lambda E$  and  $H$ , and simulated lake thermal conditions (i.e., surface temperature and heat content). The sign convention for  $\lambda E$  and  $H$  is upward positive, that is, surface heat loss or cooling is presented as positive values. SWE from NAM and CFSv2 was then evaluated with observations and examined in terms of how the simulated SWE related to the lakewide averages of  $\lambda E$  and  $H$  and cumulative evaporation, as well as what combination of algorithms and forcings among the 12 model runs would improve simulations of LES events.

Additionally, we conducted a water vapor budget analysis for NAM and CFSv2 to test if cumulative lake evaporation was large enough to account for the amount of snow precipitated during the LES event.

### c. Simulation setting of FVCOM

Version 3.2 of the FVCOM code was used to conduct the nine hydrodynamic simulations. The computational domain covers all of Lake Erie (Fig. 1) with higher resolution near the coast ( $\sim 200$  m) and coarser resolution offshore ( $\sim 3$  km), as in the next-generation NOAA Lake Erie Operational Forecast System (LEOFS; <https://tidesandcurrents.noaa.gov/ofs/leofs/leofs.html>). The total number of nodes (i.e., corners of triangular cells) and elements (i.e., center points of triangular cells) were 6106 and 11 509, respectively. The bathymetry used in the grid was derived from NOAA's 3-arc-s raster bathymetry for Lake Erie (<http://www.ngdc.noaa.gov/mgg/greatlakes/erie.html>). The model included the level-2.5 turbulence closure parameterization (Mellor and Yamada 1982), with a surface wave-breaking model as the surface boundary condition (Craig and Banner 1994). The background vertical eddy viscosity and diffusivity were set at  $10^{-6} \text{ m}^2 \text{ s}^{-1}$ . Horizontal diffusion was calculated with a Smagorinsky eddy diffusion parameterization (Smagorinsky 1963). The external and internal time steps were set at 5 and 30 s, respectively.

To evaluate the uncertainty of the modeled  $\lambda E$  and  $H$ , we tested three different meteorological forcings that drove FVCOM and three different algorithms to calculate  $\lambda E$  and  $H$  within FVCOM, yielding a total of nine FVCOM runs. The selected flux algorithms were the Coupled Ocean–Atmosphere Response Experiment (COARE)-Met Flux Algorithm (Fairall et al. 1996a,b; [https://coaps.fsu.edu/COARE/flux\\_algor/](https://coaps.fsu.edu/COARE/flux_algor/)); the method built in the Los Alamos Sea Ice Model, hereafter referred to as J99 (Jordan et al. 1999; Hunke et al. 2015); and the algorithm developed by Liu and Schwab (1987), hereafter referred to as LS87, that has been routinely used for Great Lakes modeling applications (Beletsky et al. 2006; Wang et al. 2010; Anderson and Schwab 2013; Fujisaki et al. 2013). COARE is one of the most frequently used algorithms in the air–sea interaction community and was first adopted in the official FVCOM version 2.7 (Chen et al. 2006). It was subsequently modified and validated at higher winds in the version known as COARE 3.0 (Fairall et al. 2003). The latest version, COARE 3.5 (Edson et al. 2013), includes the wave influence on the Charnock parameter (Charnock 1955), which is the ratio of the roughness length of momentum multiplied by the gravitational restoring force to the surface stress. FVCOM mostly incorporated these updates as the model was upgraded, with the exception that the latest version of



FVCOM (version 4.0) has not yet included the wave influence on the Charnock parameter. J99 and LS87 were included in FVCOM version 3 and later (Chen et al. 2013). J99 was adapted from a flux coupler in the Community Earth System Model (CESM; Jordan et al. 1999; Kauffman and Large 2002) and was also built into the code of the Los Alamos Sea Ice Model (Hunke et al. 2015). LS87 was originally developed at NOAA's Great Lakes Environmental Research Laboratory (GLERL; Liu and Schwab 1987) and was subsequently used in a variety of Great Lakes research and operational environments (Beletsky et al. 2003; Wang et al. 2010; Anderson and Schwab 2013; Rowe et al. 2015). The inclusion of LS87 in FVCOM was tied to the fact that the algorithm was historically part of real-time nowcasts and forecasts of GLOFS based on the Princeton Ocean Model and that GLOFS was also transitioning its physical model to FVCOM at the time of the study.

The three algorithms are commonly based on the Monin–Obukhov similarity theory (Obukhov 1971; Kantha and Clayson 2000). The same applies to NAM and CFSv2, where a heat flux calculation algorithm is part of the surface boundary layer parameterization. While there are minor differences in detail in the coefficients in stability functions and roughness length parameterizations (see references in Table 1), COARE has a distinct feature in that it takes convective behavior and gustiness effects into account. In addition, COARE distinguishes roughness length scales of temperature and humidity from that of momentum (Fairall et al. 1996b, 2003).

The selected meteorological forcing data were the interpolated observations (Interp), High-Resolution Rapid Refresh (HRRR; Benjamin et al. 2016a,b), and CFSv2 (Saha et al. 2014, 2010). The three meteorological forcings were applied to the model on an hourly basis by providing wind speed at 10-m height, surface air temperature, specific humidity/dewpoint/relative humidity (varied based on flux calculation algorithms), and cloud fraction. Note that HRRR and CFSv2 simulate  $\lambda E$  and  $H$  in their own atmospheric model framework, but in the FVCOM simulations, HRRR and CFSv2 provide surface meteorology instead of  $\lambda E$  and  $H$  to force FVCOM. As mentioned in section 2b, we also examined direct outputs of  $\lambda E$  and  $H$  from CFSv2; those from HRRR were not archived for the period of focus in this study and therefore were not available for our comparison.

The Interp forcing is based on surface meteorological measurements around Lake Erie. The 29 stations include those from the National Data Buoy Center (NDBC) and the Coastal Marine Automated Network. The overland observations are corrected to overlake values based on Croley (1989a,b), which includes the impacts of atmospheric stability, and the station data

are interpolated into the model grid based on an objective analysis (Schwab and Bedford 1999) with the “natural neighbor” interpolation (Beletsky et al. 2003). Along with the LS87 algorithm, the Interp forcing has been used for the Great Lakes modeling applications (Beletsky et al. 2006; Wang et al. 2010; Anderson and Schwab 2013; Fujisaki et al. 2013). The Interp forcing is similar to the LLTM forcing based on the station data. However, there are a couple of differences: 1) the LLTM forcing does not include overlake observations such as buoys, and 2) the Interp forcing only uses coastal and offshore observations and does not include overland stations far from the coastline, while the LLTM forcing includes all stations located within 50 km of the basin watershed.

HRRR is a relatively new, cloud-resolving, convection-allowing weather model with horizontal resolution of 3 km (Benjamin et al. 2016a,b) that became operational on 30 September 2014. Radar data are assimilated in the HRRR every 15 min over a 1-h period, adding further details to those provided by the hourly data assimilation from the 13-km radar-enhanced Rapid Refresh (RAP). HRRR was used as a meteorological forcing for three of the FVCOM model runs (Table 1).

All of the FVCOM runs started on 10 November 2014 and ended on 23 November 2014. The initial condition of the lake was identical for the nine runs. It was created by an annual FVCOM simulation with data assimilation of the lake surface temperature (LST), where the model's LST was nudged to the Great Lakes Surface Environmental Analysis (GLSEA; <https://coastwatch.glerl.noaa.gov/glsea/doc/>). GLSEA is the composite analysis of NOAA Advanced Very High Resolution Radiometer imagery and ice concentration maps from the National Ice Center. LSTs are updated daily using information from the cloud-free portions of the previous day's satellite imagery. If no imagery is available, a smoothing algorithm is applied to the previous day's estimate; therefore, the accuracy tends to be lower on cloudy days. To find the best start date for simulations, the LST data from GLSEA were examined with the observations at the three buoy locations. We examined several days prior to the LES events (before 17 November) and found that the LST from GLSEA showed a 2°C deviation from the 11–16 November buoy data but showed a deviation of less than 0.5°C from the buoy data on 10 November. Therefore, 10 November was selected to provide the initial condition for the nine FVCOM runs.

#### d. Eddy covariance data

Direct flux measurements at two stations in Lake Erie were used to validate modeled  $\lambda E$  and  $H$  (Fig. 1). The

PermS2 station (41.717°N, 83.267°W) is located on the City of Toledo water crib intake in the western basin of Lake Erie (Fig. 1). The 30-min raw data are publicly available on the LECSN website ([http://lees.geo.msu.edu/sensor\\_net/](http://lees.geo.msu.edu/sensor_net/)). The sensor height for the PermS2 station is 14.5 m. The Long Point Lighthouse (42.549°N, 80.049°W) is located at the end of a sand spit that extends roughly 40 km into Lake Erie from the northeast shore of the lake (Fig. 1). The platform for direct flux measurements was installed as part of GLEN following the installation of four other stations across the Great Lakes (Blanken et al. 2011; Spence et al. 2011, 2013; Lenters et al. 2013). This station has provided direct flux measurements since May 2012. The sensor height for the Long Point station is 29.5 m.

Turbulent fluxes of latent and sensible heat ( $\lambda E$  and  $H$ , respectively;  $\text{W m}^{-2}$  positive upward from the surface) were calculated from 10-Hz measurements of the vertical wind speed  $w$  ( $\text{m s}^{-1}$ ), air temperature  $T$  ( $^{\circ}\text{C}$ ), and water vapor density  $q$  ( $\text{g m}^{-3}$ ). Wind speed was measured using a 3D ultrasonic anemometer (Campbell Scientific CSAT-3), and water vapor density was measured using an open-path gas analyzer (Campbell Scientific KH20). The statistics (means and covariances) of the high-frequency data were collected and processed at 30-min intervals using a Campbell Scientific CR3000 datalogger. Corrections to the eddy covariance measurements included 2D coordinate rotations (Baldocchi et al. 1988) and corrections for air density fluctuations (Webb et al. 1980), sonic pathlength, high-frequency attenuation, and sensor separation (Massman 2000; Horst 1997). Because of the Long Point station's location along the northeastern edge of the sand spit, its measured fluxes may have been influenced by the land surface with significant altitude when the wind direction was between 230° and 270°. Therefore, data were filtered to not include these periods.

#### e. Snow water equivalent observational analysis

The Snow Data Assimilation System (SNODAS) is a modeling and data assimilation system developed by the NOAA/National Weather Service's National Operational Hydrologic Remote Sensing Center (NOHRSC) to provide the best possible estimates of snow cover and associated variables as gridded data to support hydrologic modeling and analysis (Barrett 2003). Here, the data were considered as observational analyses to compare with simulated SWE from NAM and CFSv2. The domain covers the contiguous United States, and the data are provided daily with a 1-km horizontal resolution. Although snowfall would be a more direct variable to evaluate the models' capability in reproducing an LES event, it was found that few observations of snowfall were conducted over the Buffalo metropolitan area during the

LES events, but there were a decent number of observations of SWE (National Snow Analyses; <https://www.nohrsc.noaa.gov/nsa/>) that were incorporated into the analyses. Therefore, the SWE product was chosen from SNODAS to compare with the modeled SWE by CFSv2 and NAM, as well as the modeled cumulative lake evaporation. Note that SWE is a measure of actual snow mass existing over an area; it reflects temporarily cumulative snowfall to some extent but also includes the loss of snow mass due to melting.

#### f. Water vapor budget analysis

We set a column control volume where the upper boundary was the top of the atmosphere, and the lower boundary enclosed both Lake Erie and the land area impacted by LES during the events (the region surrounded by a dashed gray line in Fig. 1). Note that the control volume covered not only the Buffalo metropolitan area, but also the entire downwind area.

The temporal change of water vapor mass in the control volume  $Q$  can be described as

$$\frac{dQ}{dt} = \int_A (e - p) dA - F_v, \quad (1)$$

where  $p$  and  $e$  are precipitation and upward water flux (i.e., evapotranspiration and sublimation) per unit surface area, respectively. Parameters  $A$  and  $dA$  are the area of the lower boundary of the control volume and the differential of it, respectively. Parameter  $F_v$  is the divergence of water vapor. Using  $P = \int_A p dA$  and  $E = \int_A e dA$ , Eq. (1) can be rewritten into

$$P = E - F_v - \frac{dQ}{dt}. \quad (2)$$

The divergence of water vapor in the control volume can be calculated as

$$F_v = \oint_{p_0}^{p_s} \frac{q}{g} \mathbf{v} \cdot \mathbf{n} dp dl, \quad (3)$$

where  $q$  is the water vapor mixing ratio,  $g$  is the gravity acceleration,  $\mathbf{v}$  is the wind vector, and  $\mathbf{n}$  is a unit normal vector to the outside of the control volume. Parameters  $p_0$  and  $p_s$  are the air pressure at the top of the atmosphere and at the lake or ground surface, respectively. The contour integral is along the gray dashed line in Fig. 1.

To evaluate the relative contribution of  $E$ ,  $F_v$ , and  $dQ/dt$  to  $P$  (i.e., how much lake evaporation contributed to precipitation in the control volume), the weather model results were used from CFSv2 and NAM to compute each component of the water vapor budget. Water vapor mixing ratios were derived with precipitable water for NAM and

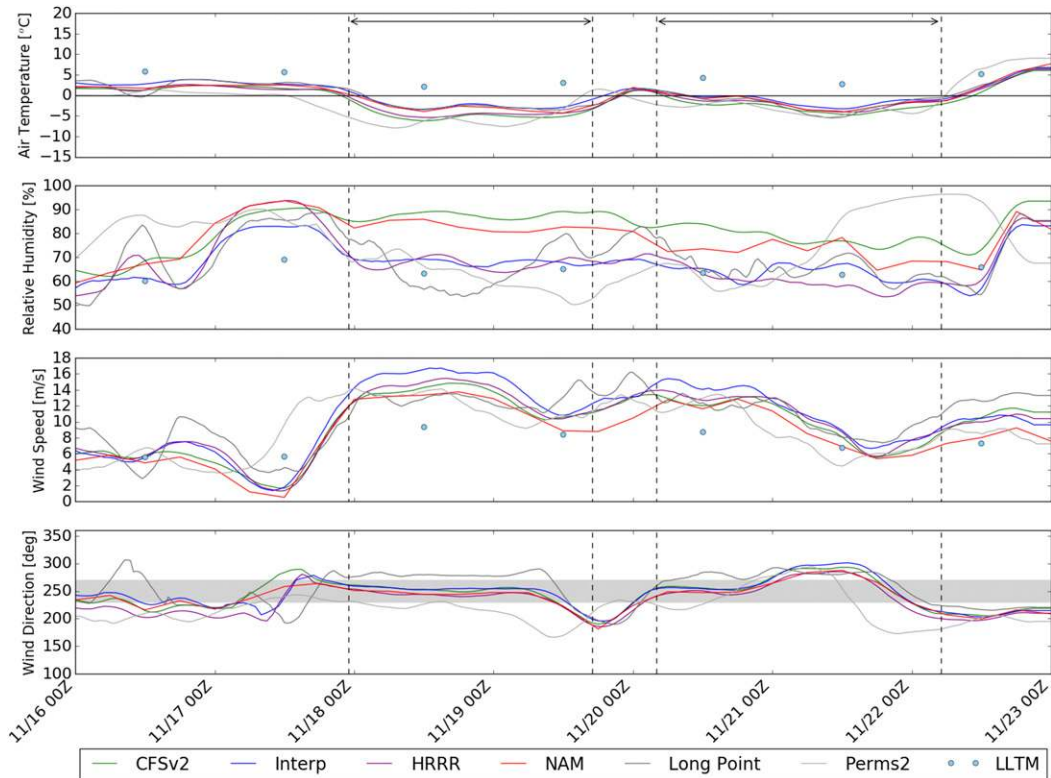


FIG. 2. Overlake surface air temperature, relative humidity, wind speed, and wind direction from the lakewide averages of meteorological datasets, CFSv2 (green line), Interp (blue line), HRRR (purple line), NAM (red line), and LLTM (light blue circles), as well as point values at the Long Point station (dark gray line) and the Perms2 station (light gray line) from 16 to 23 Nov 2014. The 6-h rolling averages are shown except for the NAM data and the LLTM data, which are 6-hourly data and daily averages, respectively. The LLTM data do not include wind direction. A horizontal line on the surface air temperature panel denotes  $0^{\circ}\text{C}$ . The shaded region on the wind direction panel denotes the range from  $230^{\circ}$  to  $270^{\circ}$ . We did not use eddy covariance data from the Long Point station when the corresponding wind direction was within this range because of overland fetch. The two periods between the dashed vertical lines denote the duration of the two storms during the LES event.

with specific humidity for CFSv2. This method is similar to the one used by Bryan et al. (2015), but differed through the inclusion of the temporal change of water vapor content due to the much shorter duration than an annual cycle.

### 3. Results and discussion

#### a. Comparison of meteorological variables

Regarding the lakewide average, the meteorological conditions (i.e., air temperature, relative humidity, wind speed and direction) were similar among the datasets during the 7-day period (Fig. 2). An exception is the LLTM forcing, whose air temperature was notably warm-biased during the period. This was likely because it did not assimilate offshore observations (e.g., buoys). The other forcings, which did assimilate offshore observations, showed reasonable agreement.

On 12 November, surface air temperature dropped sharply from  $\sim 12^{\circ}$  to  $2^{\circ}$ – $4^{\circ}\text{C}$  (except for the LLTM forcing) as the cold air associated with the southward-migrating

polar air mass arrived. On 18 November, the air temperature further decreased to range from  $-6^{\circ}$  to  $-2^{\circ}\text{C}$  as the first storm of the LES event arrived. A slight rise in surface air temperature to  $\sim 2^{\circ}\text{C}$  was seen at 0000 UTC 20 November, but as the second storm arrived, it decreased again to range from  $-4^{\circ}$  to  $-2^{\circ}\text{C}$ . This decrease was not seen in the LLTM forcing. Relative humidity during the period ranged from 50% to 95% and has more variation among the data sources compared with the other variables. Wind speed mostly remained below  $10\text{ m s}^{-1}$  with the exception of early in the day on 17 November, which saw increases to over  $15\text{ m s}^{-1}$  lasting until early the next morning. Wind speeds at the PermS2 station data showed earlier increases in the observed meteorology by  $\sim 12\text{ h}$ . All the time series showed that winds were mostly derived from the southwest during the LES events. Wind directions at the Long Point and PermS2 stations tended to be rotated by a range from  $0^{\circ}$  to  $+50^{\circ}$  and from  $-50^{\circ}$  to  $0^{\circ}$  from the lakewide averages, respectively.



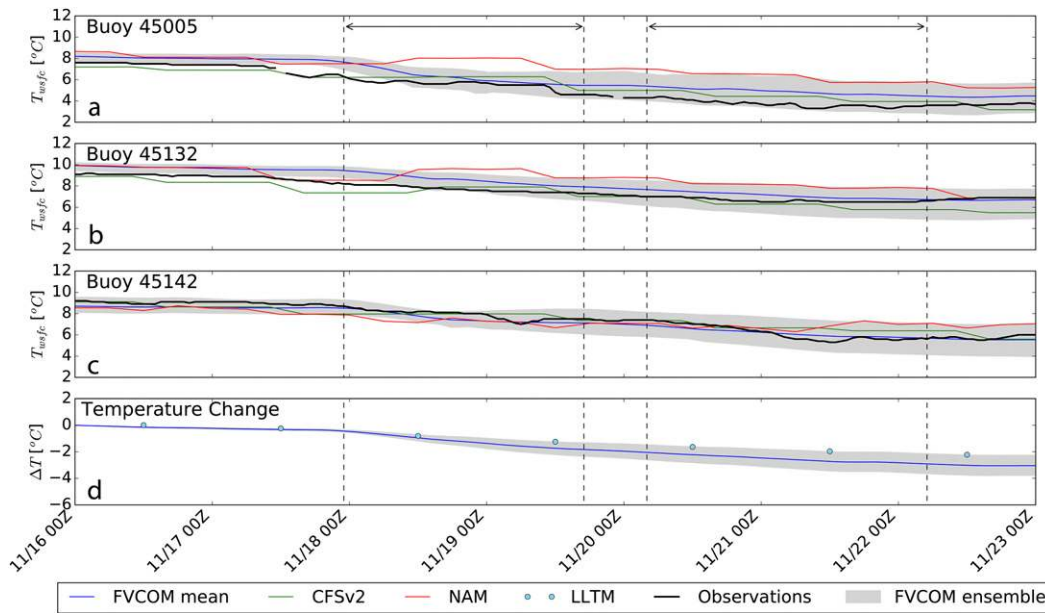


FIG. 3. Comparison of lake surface temperature  $T_{wsfc}$  at the three buoy locations (a) station 45005 in the western basin, (b) station 45132 in the central basin, and (c) station 45142 in the eastern basin, as well as (d) the change in 3D mean water temperature  $\Delta T$  beginning on 16 Nov 2014. The buoy locations are shown in Fig. 1. Simulation results are the mean (blue line) and spread (gray area) of the nine-member FVCOM-based ensemble, CFSv2 (green line), NAM (red line), and LLTM (light blue circles). Only lake surface temperature was available for the NAM and CFSv2 archive, and LLTM provides only lakewide average values. The two periods between the dashed vertical lines denote the duration of the two storms during the LES event.

*b. Comparison of lake temperatures*

We verified the simulated water temperatures in comparison with buoy measurements. Figure 3 shows the time series of LST at the three buoy sites, as well as the 3D mean water temperature, which is proportional to the lake heat content. The inflection, or steepening of slopes, at 0000 UTC 18 November corresponded to the significant heat loss (i.e., increased  $\lambda E$  and  $H$ ) during the first storm. While the models overall reproduced the temporal changes of LST observed at the buoy locations, including the inflection on 18 November, the simulation results diverged as time proceeded. This is because simulated  $\lambda E$  and  $H$ , which provide the primary cooling to the water surface, presented significant variations among the 12 models (see sections 3c and 3d). This was especially true for the FVCOM and LLTM simulations, and in NAM and CFSv2, data assimilation also played a role in restricting the simulated lake temperature. Note that 1) only lake surface temperature was available from the NAM and CFSv2 archives for comparison, and 2) because the LLTM consists of lakewide averages, it was only included in the comparison of 3D mean water temperature change.

Interestingly, even though the nine FVCOM runs started from the same initial condition, the spread of the FVCOM-simulated water temperature increased notably during the two storms, corresponding to the

variation of the peak  $\lambda E$  and  $H$  presented by the nine FVCOM runs (see sections 3c and 3d). Mean changes in 3D mean water temperature between the FVCOM and LLTM results during the first and second storms were  $-1.4^\circ$  and  $-0.8^\circ\text{C}$ , respectively, with a larger standard deviation in the first storm (Table 2). The 3D mean water temperature in the FVCOM results had a range of  $5.8^\circ\text{--}8^\circ\text{C}$  at the end of the simulation period. These lower and upper limits corresponded with the results of HRRR-LS87 and Interp-COARE, respectively. The LLTM results were warm-biased by  $\sim 3.4^\circ\text{C}$  from the FVCOM results on 10 November, and this bias continued through 23 November. The warm bias in the LLTM’s water temperature simulations is

TABLE 2. Uncertainty levels of the simulated 3D water temperature change  $\Delta T$ , peak of lake wide mean  $\lambda E$  and  $H$ , and cumulative evaporation  $\Sigma(E)$  during the two storms, represented by averages among the models and standard deviations. The first storm occurred from 2300 UTC 17 Nov to 1700 UTC 19 Nov 2014, and the second one from 0400 UTC 20 Nov to 0500 UTC 22 Nov 2014. Note that 3D water temperature change is only from the nine FVCOM and LLTM simulations.

	$\Delta T$ ( $^\circ\text{C}$ )	$\lambda E$ ( $\text{W m}^{-2}$ )	$H$ ( $\text{W m}^{-2}$ )	$\Sigma(E)$ (cm)
First storm	$-1.4 \pm 0.33$	$385 \pm 63$	$458 \pm 167$	$1.9 \pm 0.24$
Second storm	$-0.8 \pm 0.14$	$249 \pm 34$	$227 \pm 66$	$1.2 \pm 0.13$

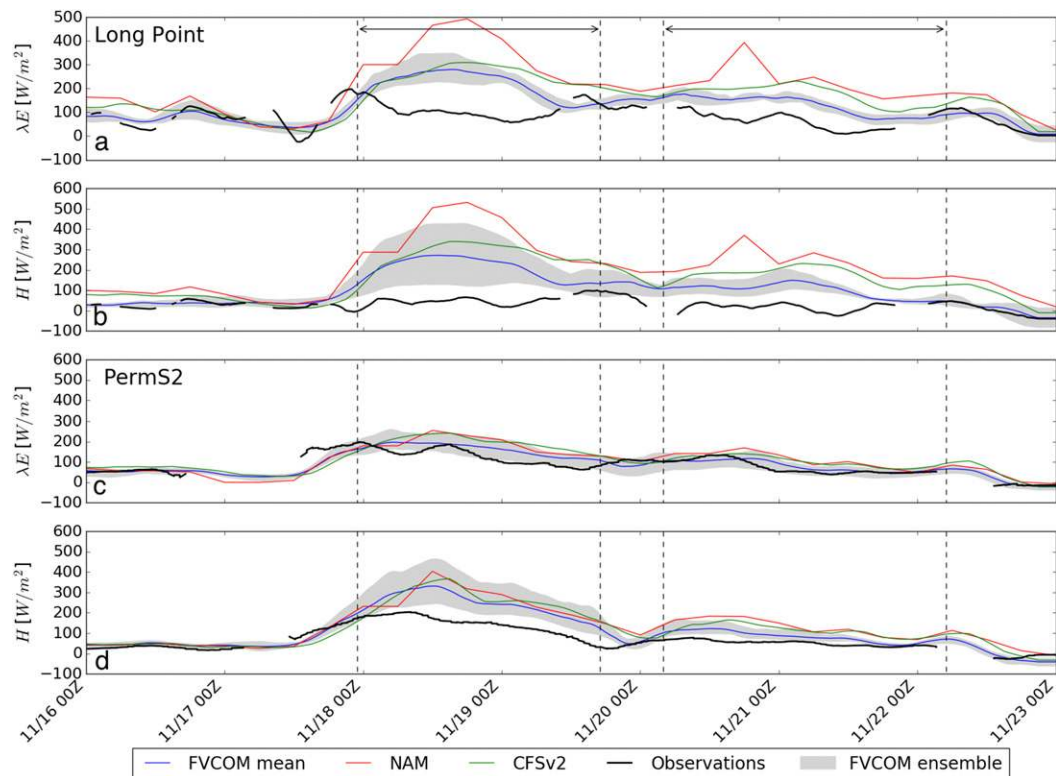


FIG. 4. Comparison between the simulated and observed (a),(c) latent  $\lambda E$  and (b),(d) sensible  $H$  heat fluxes at Long Point in (a) and (b) and Perms2 in (c) and (d). Simulation results include the mean (blue line) and spread (gray region) of the nine-member FVCOM-based ensemble, NAM (red line), and CFSv2 (green line). The 6-h averages are shown both for simulation results and observations except for NAM, whose results are instantaneous 6-hourly data. The two periods between the dashed vertical lines denote the duration of the two storms during the LES event.

likely because it did not assimilate any observed water temperature, and the air temperature in the forcing was warm-biased against the other forcing datasets during the simulation period (see section 3a).

### c. Comparison of $\lambda E$ and $H$

The time series of  $\lambda E$  and  $H$  from the model ensemble and the observations are illustrated in Fig. 4. All of the models captured the increase in the fluxes observed at the Perms2 station on 17 November, but the amplitudes varied among the models. At the Long Point station, the rise in the observed fluxes was not as significant as that at the Perms2 station. In particular, NAM and CFSv2 significantly overestimated  $\lambda E$  and  $H$ . The nine FVCOM runs were closer to the observations, but there was a noticeable overestimation from 18 to 19 November. Overall, the agreement was better at the Perms2 station, while the observed  $H$  was somewhat lower than the simulations. To quantify the model performance, the normalized root-mean-square errors (RMSEs) of  $\lambda E$  and  $H$  were calculated for the period from 16 to 23 November (Table 3). The FVCOM results appeared to have better scores than NAM and CFSv2, whose normalized RMSEs were close

to the FVCOM worst members. Among the FVCOM results, the COARE algorithm showed the best agreement with the observations on average. The LS87 algorithm was ranked as the worst in three out of the four categories; J99 was ranked as the worst for  $\lambda E$  at the Perms2 station.

Why did the FVCOM results present better agreement with the observed fluxes than NAM and CFSv2 did? There may be two reasons behind this. First, the higher spatial resolution in FVCOM allowed the model to reproduce detailed spatial heterogeneities in  $\lambda E$  and  $H$  over the lake, leading to a better representation of the fluxes at a single point. Figures 5 and 6 show the spatial patterns of  $\lambda E$  and  $H$  at 1200 UTC 18 November—a peak time of heat loss. Under such a cooling event, lower values of  $\lambda E$  and  $H$  typically occur near shore due to the area's smaller water depths and heat capacities; this leads to a faster cooling of the lake surface and a smaller air-lake temperature gradient. This was better captured by FVCOM (Figs. 5a–i and Figs. 6a–i), but was not well captured by CFSv2, NAM, and LLTM. Second, the COARE algorithm used in three of the nine FVCOM simulations had the capability to simulate  $\lambda E$  and  $H$  more accurately than the others. As described in

TABLE 3. Normalized RMSEs of  $\lambda E$  and  $H$  from 16 to 23 Nov 2014. In the FVCOM rows, a term in parentheses indicates a specific algorithm and a meteorological forcing dataset used for the member of ensemble runs.

	Long Point		PermS2	
	$\lambda E$	$H$	$\lambda E$	$H$
NAM	2.46	7.67	0.52	1.19
CFSv2	1.57	5.22	0.55	1.07
FVCOM best	1.00 (COARE-Interp)	1.79 (COARE-Interp)	0.26 (COARE-CFSv2)	0.45 (COARE-Interp)
FVCOM worst	1.44 (LS87-HRRR)	5.69 (LS87-CFSv2)	0.53 (J99-Interp)	1.49 (LS87-HRRR)
FVCOM mean	1.17	3.67	0.38	0.86

section 2c, COARE has distinguished features: it includes convective behavior and gustiness effects, and the roughness length scale parameterization for temperature and humidity is separated from that for momentum. Based on our column model study for the eddy covariance stations (U. Charusombat et al. 2017, unpublished manuscript), as well as the previous sensitivity study using a Canadian weather and hydrology model (Deacu et al. 2012), we suspect that the impacts of the roughness length scale parameterization for temperature and humidity are dominant.

We have two speculations regarding why the models overestimated the fluxes at Long Point. First, the observed fluxes at this station might have been affected by the land surface effect even though the quality control effort was made (i.e., data were removed for winds from 230° to 270°; see section 2d). Given the significant atmospheric cooling during this period and the lower heat capacity of the land surface layer than that of water column, the turbulent heat fluxes were expected to be lower over land than over water during the simulation period. The land surface influence was not considered in

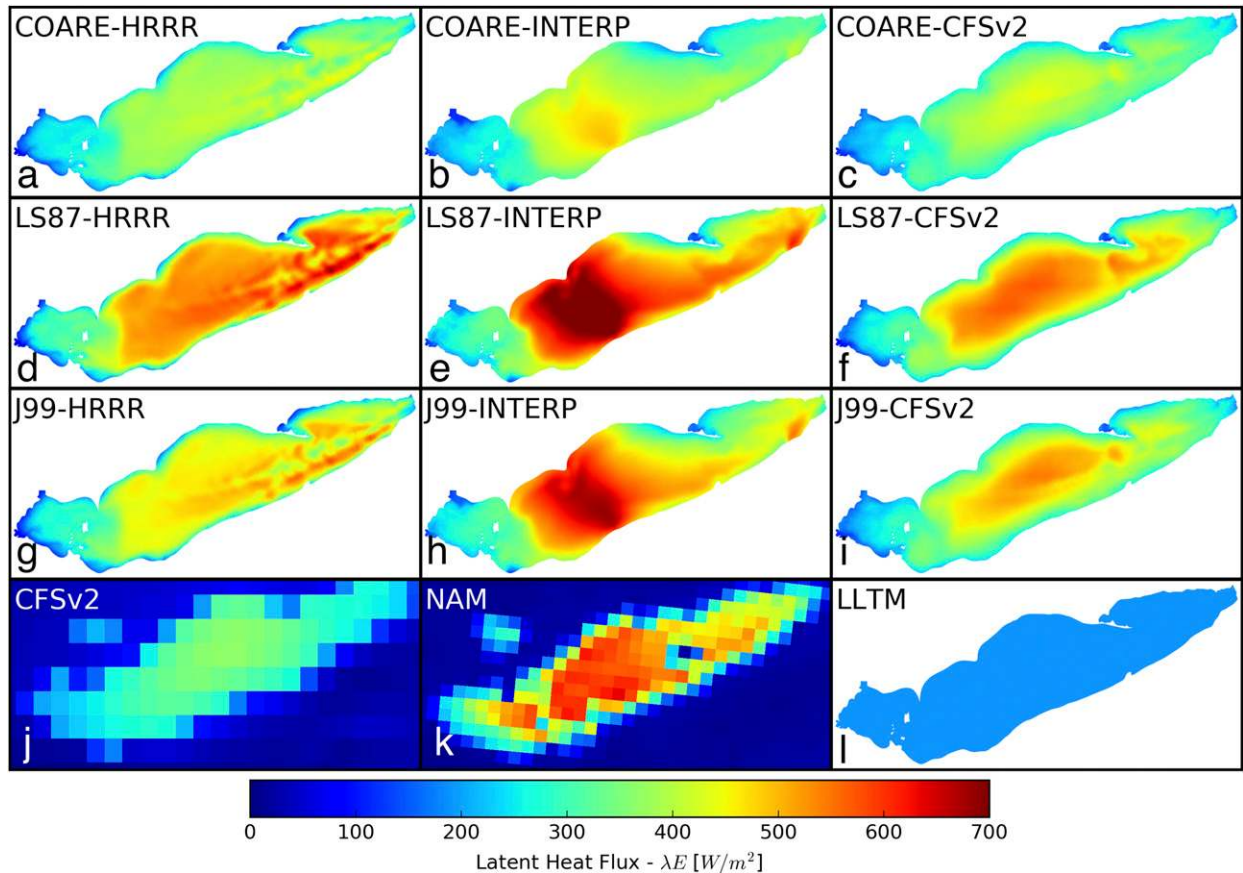


FIG. 5. Snapshots of the peak modeled latent heat flux  $\lambda E$  at 1200 UTC 18 Nov 2014. (a)–(i) Results from FVCOM. Results from (j) CFSv2, (k) NAM, and (l) LLTM. Note that the LLTM result in (l) shows the daily and lakewide average values.



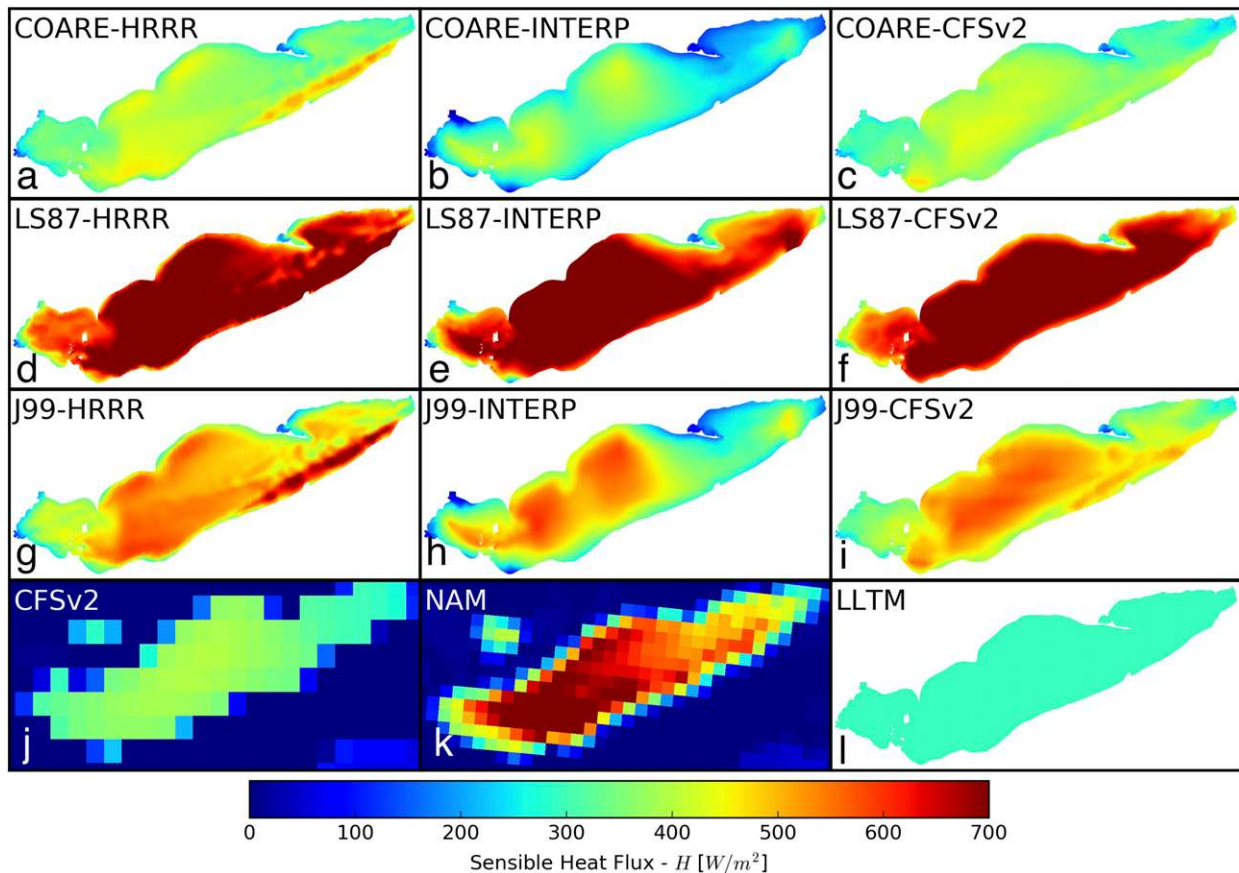


FIG. 6. As in Fig. 5, but for the sensible heat flux  $H$ .

the FVCOM and LLTM simulations. The physical models of NAM and CFSv2 have the capability to simulate the combination of overland and overwater fluxes. However, their spatial resolutions barely resolve the peninsula and shallow bathymetry. This omission of the land surface influence in the models may explain the discrepancy in the models' observations. Given that wind direction fluctuates within the averaging period of eddy covariance analysis (i.e., 30 min), removing the data with southwesterly winds might not be enough to isolate the overwater flux measurements. Second, local freezing or cooling might have occurred along the northern shore of the Long Point peninsula. Two satellite images on pre- and midstorm days indicated significantly high snowfall over the sand spit (Fig. S1 in the online supplemental material). High snowfall would have added further cooling to the water column, possibly leading to local freezing and/or ice buildup north of the station. Additional cooling or a combination of cooling and freezing could have led to a reduction of the turbulent heat fluxes by reducing the air–water temperature gradient. The ice charts of the National Ice Center for 18, 20, and 21 November 2014 did not show any ice along the peninsula.

However, it is fairly possible that the charts missed local freezing on the very near shore unless any radar imageries, visible imageries, or aircraft observations existed for the particular region.

Significant variations in the spatial patterns of  $\lambda E$  and  $H$  existed among the model results (Figs. 5 and 6). Although there were no observational data to help determine which patterns are closer to reality, the potential causes of such variations should be discussed. The magnitudes were larger overall for the FVCOM results with the LS87 and J99 algorithms and the NAM results (Figs. 5d–i,k and 6d–i,k) and lower in the FVCOM results with the COARE algorithm, the CFSv2 results, and the LLTM results (Figs. 5a–c,j,l and 6a–c,j,l). In the FVCOM results (Figs. 5a–i and 6a–i), even with the same meteorological forcing, the modeled  $\lambda E$  and  $H$  varied significantly among the different flux algorithms. It appeared that the spatial patterns of  $\lambda E$  and  $H$  were similar under the same meteorological forcing, but the fluxes are most amplified with LS87 and least amplified with COARE. The FVCOM-simulated  $\lambda E$  and  $H$  highlighted its capability in responding to submesoscale meteorological patterns over the lake such as narrow band formation and offshore convergence. For example, the



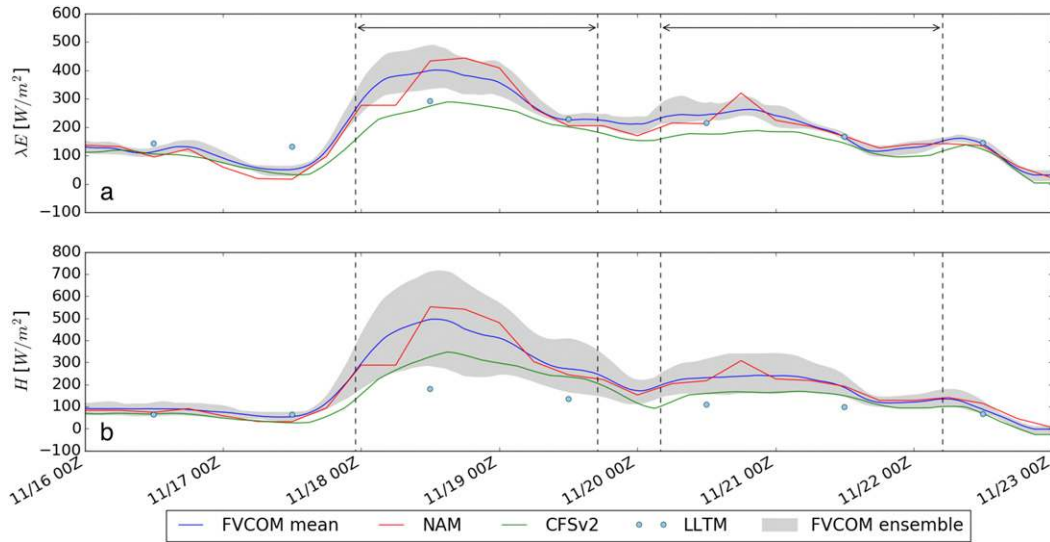


FIG. 7. Time series of the lakewide mean (a) latent  $\lambda E$  and (b) sensible  $H$  heat fluxes from the model results. Simulation results are the mean (blue line) and spread (gray area) of the nine-member FVCOM-based ensemble, NAM (red line), CFSv2 (green line), and LLTM (light blue circles). Only lake surface temperature was available for the NAM and CFSv2 archive, and LLTM provides only lakewide average values. The two periods between the dashed vertical lines denote the duration of the two storms during the LES event.

HRRR forcing included notable surface convergence in the eastern basin at 1200 UTC 18 November, which was reflected in the FVCOM simulations forced with the HRRR forcing (Figs. 5a,d,g and 6a,d,g). Though vague, a similar feature was seen in the FVCOM-simulated  $H$  with the CFSv2 forcing (Figs. 6c,i), but not the ones with the Interp forcing. The two weather model results (NAM

and CFSv2) and the LLTM results did not capture this feature. Overall, the differences in the model results were likely caused by different meteorological conditions (Fig. 2), different LSTs (Fig. 3), different spatial resolutions, and differences in the bulk flux algorithms, including stability functions and roughness length parameterization.

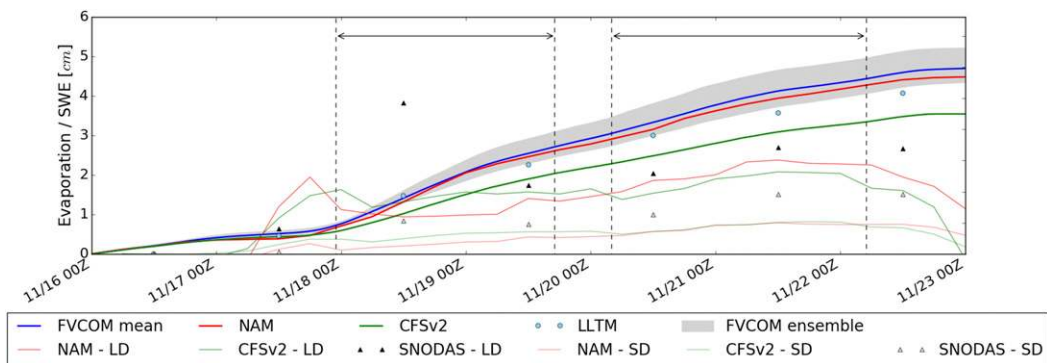


FIG. 8. Simulated lakewide cumulative evaporation and SWE. The model results of lakewide cumulative evaporation include the mean (thick blue line) and spread (gray area) of the nine-member FVCOM-based ensemble, NAM (thick red line), CFSv2 (thick green line), and LLTM (light blue circles). The SWE data include model results of NAM (thin red lines) and CFSv2 (thin green lines) and observational analysis from SNODAS (filled and outlined triangles). The SWE data are spatially integrated over the main and subdomains (Fig. 1) and normalized by the area of Lake Erie in order to be placed in the same y axis as the cumulative evaporation time series. In the legends, LD denotes integrated values over the main domain and SD denotes integrated values over the subdomain. The two periods between the dashed vertical lines denote the duration of the two storms during the LES event.

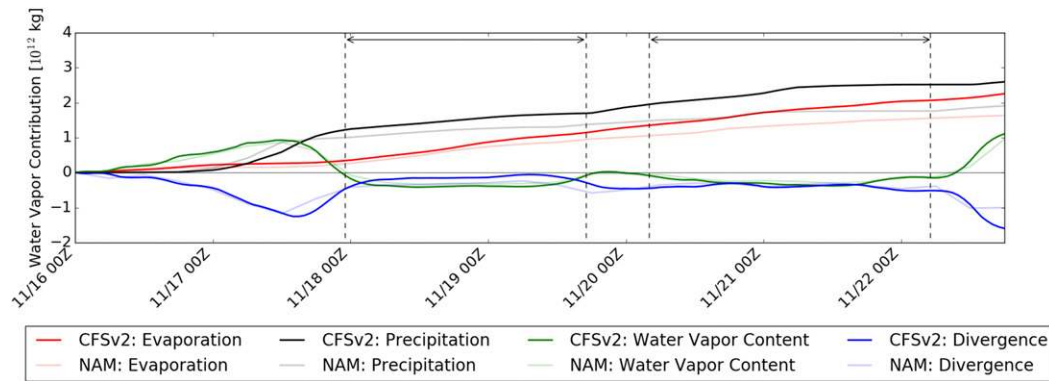


FIG. 9. Contribution of water vapor to the column control volume surrounded by a dashed line in Fig. 1. Values are integrated over time beginning at 0000 UTC 16 Nov 2014. Thin lines are from the NAM results, and thick lines are from the CFSv2 results. Red lines show the cumulative evaporation  $E$ , black lines show the cumulative precipitation  $P$ , green lines show the water vapor content  $Q$ , and blue lines show the cumulative horizontal divergence  $F_v$ . See Eq. (2) and related text for the relation of these components. The two periods between the dashed vertical lines denote the duration of the two storms during the LES event. A gray horizontal line is shown at 0 kg. Note that  $E$  and  $P$  are counted both for water and land surfaces.

#### d. Comparison of lakewide $H$ and $\lambda E$ and cumulative evaporation

The model ensemble presented notable variation in the simulated lakewide  $\lambda E$  and  $H$  and the corresponding evaporation (Figs. 7 and 8). The variation was most significant during the peak heat loss. For example, at 1200 UTC 18 November,  $H$  ranged from  $\sim 200 \text{ W m}^{-2}$  in LLTM to  $>700 \text{ W m}^{-2}$  in FVCOM ensemble members (LS87–CFSv2 and LS87–HRRR, specifically), and  $\lambda E$  ranged from  $\sim 300 \text{ W m}^{-2}$  in LLTM and CFSv2 to  $\sim 500 \text{ W m}^{-2}$  in FVCOM ensemble members (LS87–Interp, specifically). Among the non-FVCOM model outputs, the peak values of the lakewide  $\lambda E$  and  $H$  from CFSv2 and LLTM were relatively small, while those from NAM were comparable with the FVCOM mean. This could be related to the lower resolution of CFSv2 in space and of LLTM in both space and time. Uncertainty levels among the model results, represented by standard deviations, were overall larger during the first storm than during the second storm (Table 2). This corresponded to the larger standard deviations of 3D mean lake temperature change and cumulative evaporation in the first storm.

The domain for analysis was broken up into the main and subdomains, which are defined as bottom faces of the two control volumes in Fig. 1, to separately analyze the time series of cumulative evaporation and snow water equivalent during the storm period (Fig. 8). Corresponding to the spread in the lakewide  $\lambda E$  simulations, cumulative evaporations from the models presented significant variation for the 4-day duration of the two storms. Lake evaporation exceeded SWE values for both domains (Fig. 8), indicating that the lake alone

provided the air with sufficient moisture for the snowfall. To further support this conclusion, we calculated cumulative water vapor contributions of each component in Eq. (2) for the main control volume (Fig. 9). The calculation was conducted only for NAM and CFSv2, where the necessary atmospheric variables were available. During the period of interest, cumulative evaporation showed a constant increase over time in association with continuous latent heat loss from the lake. Cumulative precipitation was initiated around 1200 UTC 17 November and increased gradually in association with continuous snowfall for the rest of the period. Cumulative horizontal divergence  $\int F_v dt$  and change in water vapor content  $\Delta Q$  presented large temporal variability with similar amplitude but opposite signs. This resulted in the two terms balancing each other; for example, relatively notable convergence of net moisture (negative values of  $\int F_v dt$ ) was seen around 1800 UTC 17 November, corresponding with an increase in water vapor content by that time (increase in  $Q$ ).

Cumulative precipitation appeared to be in a primary balance with cumulative evaporation, while cumulative horizontal convergence  $-\int F_v dt$  and decrease in water

TABLE 4. Water vapor contributions to cumulative precipitation  $\int_{t_0}^{t_1} P dt$  from cumulative evaporation  $\int_{t_0}^{t_1} E dt$ , cumulative horizontal convergence  $-\int_{t_0}^{t_1} F_v dt$ , and decrease in water vapor content  $-\Delta Q$ . Parameter  $t_0$  denotes 0000 UTC 16 Nov 2014, and  $t_1$  denotes 0500 UTC 22 Nov 2014, the end of the second storm.

	$\int_{t_0}^{t_1} E dt$	$-\int_{t_0}^{t_1} F_v dt$	$\Delta Q$	Residual
NAM	88.5%	22.7%	-2.6%	-8.0%
CFSv2	81.8%	19.7%	6.9%	-8.3%

vapor content  $-\Delta Q$  also contribute by nonnegligible amounts. Table 4 shows water vapor contributions from cumulative evaporation, cumulative horizontal convergence, and a decrease in water vapor content. Residuals were due to various factors, including the use of sparse temporal snapshots (6 hourly) and round-off errors. In both models, cumulative evaporation contributed to cumulative precipitation by greater than 80%, and the  $-\int F_v dt$  term contributed around 20%. The  $-\Delta Q$  term contributed less significantly, and the ratios were similar to the residuals. Whichever terms we ascribe the residuals to, it is reasonable to conclude that lake evaporation primarily contributed to snowfall during the events. Note that this analysis was for the main control volume—the spatial resolutions of NAM and CFSv2 are too coarse to be applied to the subcontrol volume (Fig. 1). That being said, given that the subcontrol volume is part of the main control volume, it would be reasonable to speculate that lake evaporation corresponded with snowfall over the subcontrol volume as well.

How would the balance change if the evaporation component was swapped with the FVCOM-simulated  $E$ ? From the comparison of cumulative evaporation over the lake (Fig. 8), the FVCOM mean value was close to NAM. The overall balance would most likely not be changed; evaporation was a primary contributor to precipitation. On the other hand, a curious question for future work will be how FVCOM-simulated  $H$  and  $\lambda E$  could alter mesoscale condition band formation above the lake if they serve as surface boundary conditions to NAM or CFSv2.

#### e. Comparison of SWE

Here, we compared SWE simulations from NAM and CFSv2 with the observational analysis (SNODAS). The connection to the lake models, especially FVCOM, has to be speculative because none of the SWE simulations used FVCOM-simulated  $\lambda E$  and  $H$ . However, given FVCOM's better agreement with the observed  $\lambda E$  and  $H$  (section 3c) and the fact that lake evaporation contributed to the majority of snowfall (section 3d), this section includes the discussion on how the SWE simulations could be improved by using FVCOM-simulated  $\lambda E$  and  $H$ .

The modeled SWEs from CFSv2 and NAM agreed reasonably well with SNODAS for the main domain (Fig. 8). There existed an outlier in the SNODAS data on 18 November, which was likely associated with the areawide increase of SWE from 17 to 18 November and the decrease of SWE from 18 to 19 November over the southern area of Lake Erie (Fig. 10). Similar increases in SWE were found in the NAM and CFSv2 results, though

they appeared somewhat earlier compared to those in the SNODAS data. For the subdomain, both models tended to underestimate SWE from 18 to 23 November. This underestimated SWE was tied with the performance of NAM and CFSv2 in simulating the spatial fields of SWE (Fig. 10). The SNODAS showed increases of SWE along the east of Lake Erie from 17 to 18 November, associated with the snowband in the first storm, and locally concentrated SWE around the Buffalo metropolitan area on 19 November, associated with the second storm. This locally concentrated SWE remained throughout the next several days. These increases of SWE were somewhat captured by the NAM and CFSv2, but both failed to capture the intensity of SWE observed in the Buffalo metropolitan area.

NAM and CFSv2 successfully reproduced the SWE during the LES events over the main domain of  $\sim 400$  km longitudinal scale but underestimated it over the subdomain at a longitudinal scale of  $\sim 30$  km. This discrepancy could be caused by various factors in the models other than turbulent heat fluxes from the lake surface, including microphysics parameterization, horizontal grid sizes, and planetary boundary layer parameterizations. Each of these factors differs between NAM and CFSv2 (Table 1). Reeves and Dawson (2013) found that choice of microphysics parameterization could result in notable differences in simulated precipitation during an LES event; they did not confirm which parameters were superior because of a lack of observations. Undoubtedly, spatial resolution in a weather model is important. The grid size was 12 km in NAM and  $0.2^\circ$  ( $\sim 17$  km) in CFSv2. These grid sizes would not be small enough to resolve the locally concentrated snowfall in the subdomain. Conrick et al. (2015) tested various planetary and surface boundary layer parameterizations. They found that change in simulated precipitation was due to different sensible heat and moisture (proportional to latent heat) fluxes in surface boundary layer parameterizations (i.e., turbulent heat flux modeling).

It is beyond the scope of this study to determine which factor was responsible for the error in the simulated SWE fields. However, given the spread of turbulent heat fluxes among the models (sections 3c and 3d), as well as the findings of Conrick et al. (2015), it is important to discuss which alternative to turbulent heat flux modeling from the lake surface could reduce the discrepancy in the SWE fields between the simulations and SNODAS. At the eddy covariance stations, FVCOM, specifically members using the COARE algorithm, performed better than the other models. One possible way to improve SWE simulations could be through using the COARE algorithm within NAM and



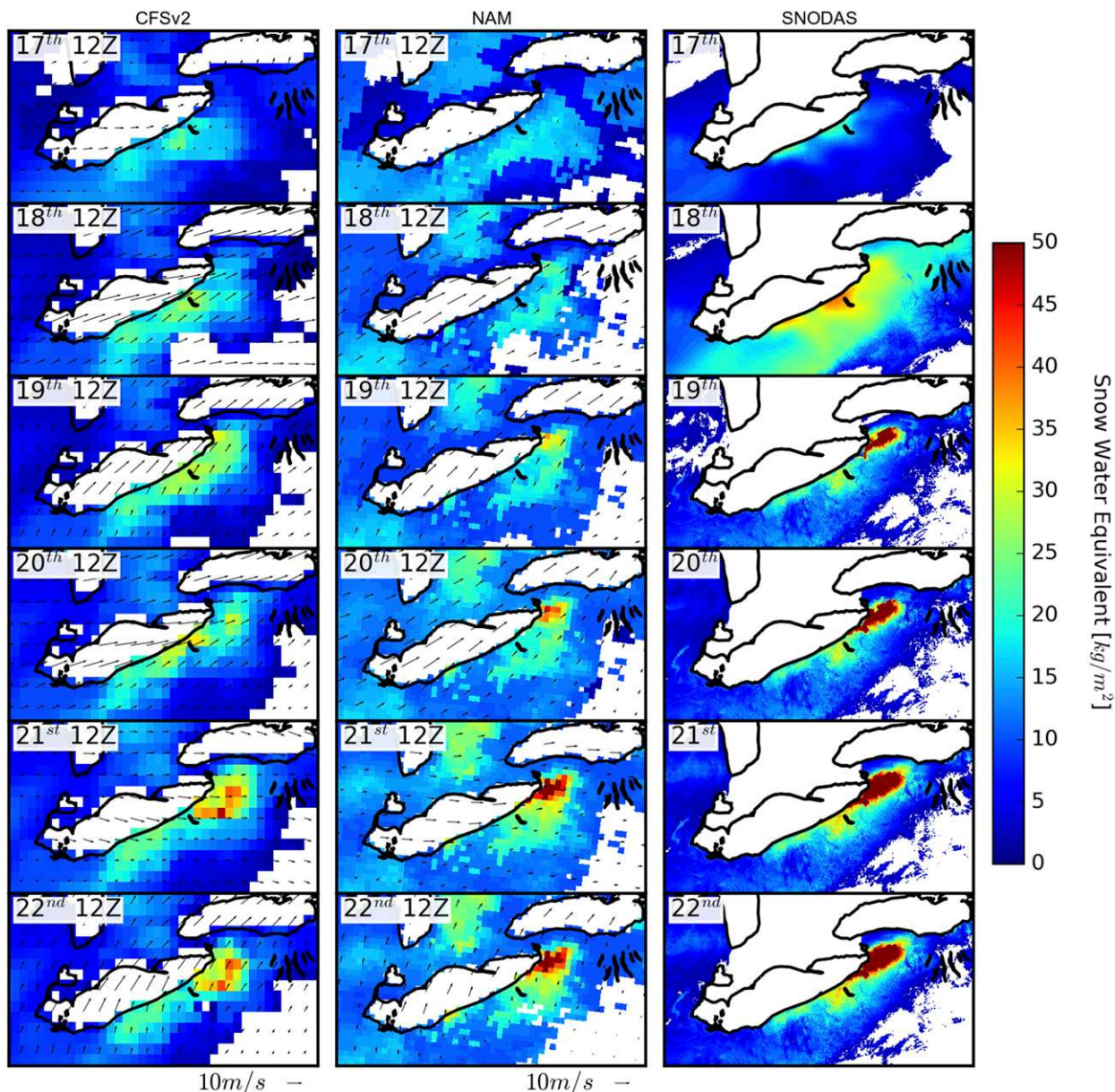


FIG. 10. SWE from the model results of NAM and CFSv2, as well as the analyses of SNODAS from 17 to 22 Nov 2014. The NAM and CFSv2 data show snapshots at 1200 UTC on each day, while the SNODAS data show a daily field. Vectors on the NAM and CFSv2 fields show daily averaged winds at 10-m height from the two models.

CFSv2 or another model with higher spatial resolution (e.g., HRRR). An alternative would be through using direct outputs of  $\lambda E$  and  $H$  from LEOFS (operational implementation of FVCOM for Lake Erie; section 2c). This allows the weather models to take advantage of detailed spatial patterns over the lake simulated in FVCOM, as higher spatial resolution is desirable for a weather model. In this sense, HRRR—whose horizontal resolution is 3 km—is an ideal model to conduct such a sensitivity study in a quasi-operational

environment. Using FVCOM-simulated  $\lambda E$  and  $H$  as surface boundary conditions in experimental HRRR simulations could be interesting to include as part of a future sensitivity study on improving LES forecasting capabilities.

#### 4. Conclusions

Numerical weather and lake models were tested by comparing outputs to observations including direct flux



measurements and a snow water equivalent analysis for the November 2014 LES event. The purposes of this study were to conduct the first-ever evaluation of simulated turbulent heat fluxes over Lake Erie in comparison with direct flux measurements, as well as to evaluate the uncertainties in simulated  $\lambda E$  and  $H$  among the models and to provide insights on what alternative models could improve LES forecasts by providing surface boundary conditions of the turbulent heat fluxes. All of the models captured the temporal variations of  $\lambda E$  and  $H$ , but the peak values varied significantly among the models. The FVCOM ensemble members, especially the ones using the COARE algorithm, presented the best agreement with the eddy covariance measurements. This was likely due to the FVCOM's capability in simulating detailed spatial patterns of  $\lambda E$  and  $H$ , as well as the COARE algorithm's more realistic treatments for the surface boundary layer physics. The water vapor budget analysis showed that a majority of snowfall during this event was attributed to lake evaporation, underscoring the importance of proper modeling of the overlake  $\lambda E$  and  $H$ . As weather models move toward higher spatial resolutions, it is important for improved LES forecasts that the surface boundary layer modeling over the lake incorporates an accurate bulk flux algorithm and submesoscale air-lake interactions. The comparison suggests that FVCOM is one of the lake models that possesses such capabilities and that the model may be a part of next-generation weather models, either by providing the turbulent heat fluxes as surface boundary conditions or by being coupled with weather or regional climate models (e.g., Xue et al. 2016).

The variation of modeled  $\lambda E$  and  $H$  resulted in the spread of water temperatures and cumulative evaporation among the models during the 4-day duration of two storms between 17 and 21 November. This divergence was a symptom of model uncertainty and was large enough to impact longer-term simulations beyond the period of the LES event. This further emphasizes the importance of accurate simulation of  $\lambda E$  and  $H$  in such a short-duration but extreme event, not only for accurate LES forecasts but also for reducing the uncertainty in longer-term simulations of seasonal ice forecasts and water balance predictions. Finally, there is a need for models that can accurately simulate water and heat loss, not just for Lake Erie but also for all the Great Lakes, on both a meteorological scale and for long-term water balance estimates (Gronewold and Stow 2014). Continued monitoring of the turbulent heat fluxes at the offshore stations is critical for such models to be evaluated and improved.

*Acknowledgments.* This research is funded by the U.S. Environmental Protection Agency's Great Lakes

Restoration Initiative (GLRI) and NOAA's Coastal Storms Program, awarded to the Cooperative Institute for Great Lakes Research (CIGLR) through the NOAA Cooperative Agreement with the University of Michigan (NA12OAR4320071). This is GLERL contribution 1861 and CILER contribution 1114. We thank Dr. Stan Benjamin at NOAA/ESRL for providing the meteorological data from HRRR, Tim Hunter at NOAA/GLERL for providing the LLTM simulation results, Dr. Yihua Hu at NCEP/EMC for providing the information on NAM specifications, and Drs. Philip Chu, Derek Posselt, and David Schwab for helpful discussion on the weather models and the flux data. The data used in this research were kindly provided by the Great Lakes Evaporation Network (GLEN) and the Lake Erie Center Sensor Network (LECSN). The GLEN data compilation and publication was provided by Limno-Tech under Award/Contract No. 10042-400759 from the International Joint Commission (IJC) through a subcontract with the Great Lakes Observing System (GLOS). The original data at the Perms2 station used for this paper are available at the LECSN website ([http://lees.geo.msu.edu/sensor\\_net/](http://lees.geo.msu.edu/sensor_net/)). The statements, findings, conclusions, and recommendations are those of the author(s) and do not reflect the views of GLEN, LimnoTech, the IJC, GLOS, or LECSN. The SNODAS data were obtained at the National Snow and Ice Data Center website (<http://dx.doi.org/10.7265/N5TB14TC>).

#### REFERENCES

- Aligo, E., B. Ferrier, G. Thompson, J. Carley, E. Rogers, and G. DiMego, 2017: The new Ferrier-Aligo microphysics in the NCEP 3-km NAM nest. *28th Conf. on Weather Analysis and Forecasting/24th Conf. on Numerical Weather Prediction*, Seattle, WA, Amer. Meteor. Soc., 4B.4, <https://ams.confex.com/ams/97Annual/webprogram/Paper314346.html>.
- Anderson, E. J., and D. J. Schwab, 2013: Predicting the oscillating bi-directional exchange flow in the Straits of Mackinac. *J. Great Lakes Res.*, **39**, 663–671, <https://doi.org/10.1016/j.jglr.2013.09.001>.
- Baldocchi, D., B. B. Hicks, and T. Meyers, 1988: Measuring biosphere-atmosphere exchanges of biologically related gases with micrometeorological methods. *Ecology*, **69**, 1331–1340, <https://doi.org/10.2307/1941631>.
- Barrett, A. P., 2003: National Operational Hydrologic Remote Sensing Center Snow Data Assimilation System (SNODAS) products at NSIDC. NSDIC Special Rep. 11, 19 pp., [https://nsidc.org/sites/nsidc.org/files/files/nsidc\\_special\\_report\\_11.pdf](https://nsidc.org/sites/nsidc.org/files/files/nsidc_special_report_11.pdf).
- Beletsky, D., D. J. Schwab, P. J. Roebber, M. J. McCormick, G. S. Miller, and J. H. Saylor, 2003: Modeling wind-driven circulation during the March 1998 sediment resuspension event in Lake Michigan. *J. Geophys. Res.*, **108**, 3038, <https://doi.org/10.1029/2001JC001159>.
- , —, and M. McCormick, 2006: Modeling the 1998–2003 summer circulation and thermal structure in Lake Michigan. *J. Geophys. Res.*, **111**, C10010, <https://doi.org/10.1029/2005JC003222>.

- Benjamin, S. G., and Coauthors, 2016a: A North American hourly assimilation and model forecast cycle: The rapid refresh. *Mon. Wea. Rev.*, **144**, 1669–1694, <https://doi.org/10.1175/MWR-D-15-0242.1>.
- , J. M. Brown, and T. G. Smirnova, 2016b: Explicit precipitation-type diagnosis from a model using a mixed-phase bulk cloud-precipitation microphysics parameterization. *Wea. Forecasting*, **31**, 609–619, <https://doi.org/10.1175/WAF-D-15-0136.1>.
- Blanken, P. D., C. Spence, N. Hedstrom, and J. D. Lenters, 2011: Evaporation from Lake Superior: 1. Physical controls and processes. *J. Great Lakes Res.*, **37**, 707–716, <https://doi.org/10.1016/j.jglr.2011.08.009>.
- Bryan, A. M., A. L. Steiner, and D. J. Posselt, 2015: Regional modeling of surface–atmosphere interactions and their impact on Great Lakes hydroclimate. *J. Geophys. Res. Atmos.*, **120**, 1044–1064, <https://doi.org/10.1002/2014JD022316>.
- Charnock, H., 1955: Wind stress on a water surface. *Quart. J. Roy. Meteor. Soc.*, **81**, 639–640, <https://doi.org/10.1002/qj.49708135027>.
- Chen, C., R. C. Beardsley, and G. Cowles, 2006: An unstructured grid, Finite-Volume Coastal Ocean Model (FVCOM) system. *Oceanography*, **19**, 78–89, <https://doi.org/10.5670/oceanog.2006.92>.
- , and Coauthors, 2013: An unstructured grid, Finite-Volume Coastal Ocean Model: FVCOM User Manual. University of Massachusetts Dartmouth School of Marine Sciences Tech. Rep. SMAST/UMASSD-13-0701, 416 pp.
- Conrick, R., H. D. Reeves, and S. Zhong, 2015: The dependence of QPF on the choice of boundary- and surface-layer parameterization for a lake-effect snowstorm. *J. Appl. Meteor. Climatol.*, **54**, 1177–1190, <https://doi.org/10.1175/JAMC-D-14-0291.1>.
- Cordeira, J. M., and N. F. Laird, 2008: The influence of ice cover on two lake-effect snow events over Lake Erie. *Mon. Wea. Rev.*, **136**, 2747–2763, <https://doi.org/10.1175/2007MWR2310.1>.
- Craig, P. D., and M. L. Banner, 1994: Modeling wave-enhanced turbulence in the ocean surface layer. *J. Phys. Oceanogr.*, **24**, 2546–2559, [https://doi.org/10.1175/1520-0485\(1994\)024<2546:MWETIT>2.0.CO;2](https://doi.org/10.1175/1520-0485(1994)024<2546:MWETIT>2.0.CO;2).
- Croley, T. E., 1989a: Verifiable evaporation modeling on the Laurentian Great Lakes. *Water Resour. Res.*, **25**, 781–792, <https://doi.org/10.1029/WR025i005p00781>.
- , 1989b: Lumped modeling of Laurentian Great Lakes evaporation, heat storage, and energy fluxes for forecasting and simulation. NOAA Tech. Memo ERL GLERL-70, 54 pp.
- , and R. A. Assel, 2002: Great Lakes evaporation model sensitivities and errors. *2nd Federal Interagency Hydrologic Modeling Conf.*, Las Vegas, NV, Subcommittee on Hydrology of the Interagency Advisory Committee on Water Data, 1–12.
- Deacu, D., V. Fortin, E. Klyszajko, C. Spence, and P. D. Blanken, 2012: Predicting the net basin supply to the Great Lakes with a hydrometeorological model. *J. Hydrometeorol.*, **13**, 1739–1759, <https://doi.org/10.1175/JHM-D-11-0151.1>.
- Edson, J. B., and Coauthors, 2013: On the exchange of momentum over the open ocean. *J. Phys. Oceanogr.*, **43**, 1589–1610, <https://doi.org/10.1175/JPO-D-12-0173.1>.
- Fairall, C. W., E. F. Bradley, J. S. Godfrey, G. A. Wick, J. B. Edson, and G. S. Young, 1996a: Cool-skin and warm-layer effects on sea surface temperature. *J. Geophys. Res.*, **101**, 1295–1308, <https://doi.org/10.1029/95JC03190>.
- , —, D. P. Rogers, J. B. Edson, and G. S. Young, 1996b: Bulk parameterization of air–sea fluxes for tropical ocean–global atmosphere Coupled Ocean–Atmosphere Response Experiment. *J. Geophys. Res.*, **101**, 3747–3764, <https://doi.org/10.1029/95JC03205>.
- , —, J. E. Hare, A. A. Grachev, and J. B. Edson, 2003: Bulk parameterization of air–sea fluxes: Updates and verification for the COARE algorithm. *J. Climate*, **16**, 571–591, [https://doi.org/10.1175/1520-0442\(2003\)016<0571:BPOASF>2.0.CO;2](https://doi.org/10.1175/1520-0442(2003)016<0571:BPOASF>2.0.CO;2).
- Fujisaki, A., J. Wang, X. Bai, G. Leshkevich, and B. Lofgren, 2013: Model-simulated interannual variability of Lake Erie ice cover, circulation, and thermal structure in response to atmospheric forcing, 2003–2012. *J. Geophys. Res. Oceans*, **118**, 4286–4304, <https://doi.org/10.1002/jgrc.20312>.
- Gronewold, A. D., and C. A. Stow, 2014: Water loss from the Great Lakes. *Science*, **343**, 1084–1085, <https://doi.org/10.1126/science.1249978>.
- , and Coauthors, 2015: Impacts of extreme 2013–2014 winter conditions on Lake Michigan’s fall heat content, surface temperature, and evaporation. *Geophys. Res. Lett.*, **42**, 3364–3370, <https://doi.org/10.1002/2015GL063799>.
- Hjelmfelt, M. R., 1990: Numerical study of the influence of environmental conditions on lake-effect snowstorms over Lake Michigan. *Mon. Wea. Rev.*, **118**, 138–150, [https://doi.org/10.1175/1520-0493\(1990\)118<0138:NSOTIO>2.0.CO;2](https://doi.org/10.1175/1520-0493(1990)118<0138:NSOTIO>2.0.CO;2).
- Horst, T. W., 1997: A simple formula for attenuation of eddy fluxes measured with first-order-response scalar sensors. *Bound.-Layer Meteorol.*, **82**, 219–233, <https://doi.org/10.1023/A:1000229130034>.
- Hunke, E. C., W. H. Lipscomb, A. K. Turner, N. Jeffery, and S. Elliott, 2015: CICE: The Los Alamos sea ice model documentation and software user’s manual version 5.1. Los Alamos National Laboratory Tech Rep. LA-CC-06-012, 115 pp.
- Hunter, T. S., A. H. Clites, K. B. Campbell, and A. D. Gronewold, 2015: Development and application of a North American Great Lakes hydrometeorological database—Part I: Precipitation, evaporation, runoff, and air temperature. *J. Great Lakes Res.*, **41**, 65–77, <https://doi.org/10.1016/j.jglr.2014.12.006>.
- Janjić, Z., and R. Gall, 2012: Scientific documentation of the NCEP nonhydrostatic multiscale model on the B grid (NMMB). Part 1 Dynamics. NCAR Tech. Note NCAR/TN-489+STR, 75 pp., <https://doi.org/10.5065/D6WH2MZX>.
- Jordan, R. E., E. L. Andreas, and A. P. Makshtas, 1999: Heat budget of snow-covered sea ice at North Pole 4. *J. Geophys. Res.*, **104**, 7785–7806, <https://doi.org/10.1029/1999JC900011>.
- Kantha, L. H., and C. A. Clayson, 2000: Surface exchange processes. *Small Scale Processes in Geophysical Fluid Flows*, L. H. Kantha and C. A. Clayson, Eds., International Geophysics Series, Vol. 67, Academic Press, 417–509.
- Kauffman, B. G., and W. G. Large, 2002: The CCSM coupler, version 5.0.1. Tech. Doc., 47 pp., [http://www.cesm.ucar.edu/models/ccsm2.0.1/cpl5/users\\_guide.pdf](http://www.cesm.ucar.edu/models/ccsm2.0.1/cpl5/users_guide.pdf).
- Kristovich, D. A. R., and N. F. Laird, 1998: Observations of widespread lake-effect cloudiness: Influences of lake surface temperature and upwind conditions. *Wea. Forecasting*, **13**, 811–821, [https://doi.org/10.1175/1520-0434\(1998\)013<0811:OOWLEC>2.0.CO;2](https://doi.org/10.1175/1520-0434(1998)013<0811:OOWLEC>2.0.CO;2).
- , —, and M. R. Hjelmfelt, 2003: Convective evolution across Lake Michigan during a widespread lake-effect snow event. *Mon. Wea. Rev.*, **131**, 643–655, [https://doi.org/10.1175/1520-0493\(2003\)131<0643:CEALMD>2.0.CO;2](https://doi.org/10.1175/1520-0493(2003)131<0643:CEALMD>2.0.CO;2).
- , and Coauthors, 2016: The Ontario Winter Lake-effect Systems (OWLeS) field campaign. *Bull. Amer. Meteor. Soc.*, **98**, 315–332, <https://doi.org/10.1175/BAMS-D-15-00034.1>.
- Lenters, J. D., J. B. Anderson, P. D. Blanken, C. Spence, and A. E. Suyker, 2013: Assessing the impacts of climate variability and change on Great Lakes evaporation: Implications for water levels and the need for a coordinated observation

- network. GLISA 2011 Project Rep., D. Brown, D. Bidwell, and L. Briley, Eds., 11 pp., [http://glisa.umich.edu/media/files/projectreports/GLISA\\_ProjRep\\_Lake\\_Evaporation.pdf](http://glisa.umich.edu/media/files/projectreports/GLISA_ProjRep_Lake_Evaporation.pdf).
- Liu, P. C., and D. J. Schwab, 1987: A comparison of methods for estimating  $u_*$  from given  $u_z$  and air-sea temperature differences. *J. Geophys. Res.*, **92**, 6488–6494, <https://doi.org/10.1029/JC092iC06p06488>.
- Łobocki, L., 1993: A procedure for the derivation of surface-layer bulk relationships from simplified second-order closure models. *J. Appl. Meteor.*, **32**, 126–138, [https://doi.org/10.1175/1520-0450\(1993\)032<0126:APFTDO>2.0.CO;2](https://doi.org/10.1175/1520-0450(1993)032<0126:APFTDO>2.0.CO;2).
- Long, P. E., 1986: An economical and compatible scheme for parameterizing the stable surface layer in the medium range forecast model. NCEP Office Note 321, 24 pp., <http://www.lib.ncep.noaa.gov/ncepofficenotes/files/01408602.pdf>.
- , 1990: Derivation and suggested method of the application of simplified relations for surface fluxes in the medium-range forecast model: Unstable case. NCEP Office Note 356, 53 pp., <http://www.lib.ncep.noaa.gov/ncepofficenotes/files/0140893E.pdf>.
- Massman, W. J., 2000: A simple method for estimating frequency response corrections for eddy covariance systems. *Agric. For. Meteorol.*, **104**, 185–198, [https://doi.org/10.1016/S0168-1923\(00\)00164-7](https://doi.org/10.1016/S0168-1923(00)00164-7).
- Mellor, G. L., and T. Yamada, 1982: Development of a turbulent closure model for geophysical fluid problems. *Rev. Geophys.*, **20**, 851–875, <https://doi.org/10.1029/RG020i004p00851>.
- Moorthi, S., R. Sun, H. Xiao, and R. C. Mechoso, 2016: Southeast Pacific low-cloud simulation in the NCEP GFS: Role of vertical mixing and shallow convection. NCEP Office Note 463, 28 pp., <http://www.lib.ncep.noaa.gov/ncepofficenotes/files/on463.pdf>.
- Nason, G., 2014: November 2014's lake-effect snowstorms. *Buffalo News*, 5 December.
- National Weather Service, 2014a: Lake effect summary, November 17–19, 2014. Buffalo, NY, Weather Forecast Office, [http://www.weather.gov/buf/lake1415\\_stormb.html](http://www.weather.gov/buf/lake1415_stormb.html).
- , 2014b: Lake effect summary, November 19–21, 2014. Buffalo, NY, Weather Forecast Office, [http://www.weather.gov/buf/lake1415\\_stormc.html](http://www.weather.gov/buf/lake1415_stormc.html).
- Niziol, T. A., W. R. Snyder, and J. S. Waldstreicher, 1995: Winter weather forecasting throughout the eastern United States. Part IV: Lake effect snow. *Wea. Forecasting*, **10**, 61–77, [https://doi.org/10.1175/1520-0434\(1995\)010<0061:WWFTE>2.0.CO;2](https://doi.org/10.1175/1520-0434(1995)010<0061:WWFTE>2.0.CO;2).
- Notaro, M., A. Zarrin, S. Vavrus, and V. Bennington, 2013: Simulation of heavy lake-effect snowstorms across the Great Lakes basin by RegCM4: Synoptic climatology and variability. *Mon. Wea. Rev.*, **141**, 1990–2014, <https://doi.org/10.1175/MWR-D-11-00369.1>.
- Obukhov, A. M., 1971: Turbulence in an atmosphere with a non-uniform temperature. *Bound.-Layer Meteorol.*, **2**, 7–29, <https://doi.org/10.1007/BF00718085>.
- Ouyang, Z., C. Shao, H. Chu, R. Becker, T. Bridgeman, C. Stepien, R. John, and J. Chen, 2017: The effect of algal blooms on carbon emissions in western Lake Erie: An integration of remote sensing and eddy covariance measurements. *Remote Sens.*, **9**, 44, <https://doi.org/10.3390/rs9010044>.
- Reeves, H. D., and D. T. Dawson, 2013: The dependence of QPF on the choice of microphysical parameterization for lake-effect snowstorms. *J. Appl. Meteor. Climatol.*, **52**, 363–377, <https://doi.org/10.1175/JAMC-D-12-019.1>.
- Rogers, E., and Coauthors, 2009: The NCEP North American Mesoscale modeling system: Recent changes and future plans. *23rd Conf. on Weather Analysis and Forecasting/19th Conf. on Numerical Weather Prediction*, Omaha, NE, Amer. Meteor. Soc., 2A.4, [https://ams.confex.com/ams/23WAF19NWP/techprogram/paper\\_154114.htm](https://ams.confex.com/ams/23WAF19NWP/techprogram/paper_154114.htm).
- Rowe, M. D., E. J. Anderson, J. Wang, and H. A. Vanderploeg, 2015: Modeling the effect of invasive quagga mussels on the spring phytoplankton bloom in Lake Michigan. *J. Great Lakes Res.*, **41**, 49–65, <https://doi.org/10.1016/j.jglr.2014.12.018>.
- Saha, S., and Coauthors, 2010: The NCEP Climate Forecast System Reanalysis. *Bull. Amer. Meteor. Soc.*, **91**, 1015–1057, <https://doi.org/10.1175/2010BAMS3001.1>.
- , and Coauthors, 2014: The NCEP Climate Forecast System version 2. *J. Climate*, **27**, 2185–2208, <https://doi.org/10.1175/JCLI-D-12-00823.1>.
- Schwab, D. J., and K. W. Bedford, 1999: The Great Lakes Forecasting System. *Coastal Ocean Prediction*, C. N. K. Mooers, Ed., Coastal and Estuarine Studies, Vol. 56, Amer. Geophys. Union, 157–173.
- Shao, C., and Coauthors, 2015: Diurnal to annual changes in latent, sensible heat, and CO<sub>2</sub> fluxes over a Laurentian Great Lake: A case study in western Lake Erie. *J. Geophys. Res. Biogeosci.*, **120**, 1587–1604, <https://doi.org/10.1002/2015JG003025>.
- Skamarock, W. C., and Coauthors, 2008: A description of the Advanced Research WRF version 3. NCAR Tech. Note NCAR/TN-475+STR, 113 pp., <https://doi.org/10.5065/D68S4MVH>.
- Smagorinsky, J., 1963: General circulation experiments with the primitive equations. *Mon. Wea. Rev.*, **91**, 99–164, [https://doi.org/10.1175/1520-0493\(1963\)091<0099:GCEWTP>2.3.CO;2](https://doi.org/10.1175/1520-0493(1963)091<0099:GCEWTP>2.3.CO;2).
- Smith, A., N. Lott, and R. Vose, 2011: The integrated surface database: Recent developments and partnerships. *Bull. Amer. Meteor. Soc.*, **92**, 704–708, <https://doi.org/10.1175/2011BAMS3015.1>.
- Spence, C., P. D. Blanken, N. Hedstrom, V. Fortin, and H. Wilson, 2011: Evaporation from Lake Superior. 2: Spatial distribution and variability. *J. Great Lakes Res.*, **37**, 717–724, <https://doi.org/10.1016/j.jglr.2011.08.013>.
- , —, J. D. Lenters, and N. Hedstrom, 2013: The importance of spring and autumn atmospheric conditions for the evaporation regime of Lake Superior. *J. Hydrometeorol.*, **14**, 1647–1658, <https://doi.org/10.1175/JHM-D-12-0170.1>.
- Vavrus, S., M. Notaro, and A. Zarrin, 2013: The role of ice cover in heavy lake-effect snowstorms over the Great Lakes Basin as simulated by RegCM4. *Mon. Wea. Rev.*, **141**, 148–165, <https://doi.org/10.1175/MWR-D-12-00107.1>.
- Wang, J., H. Hu, D. Schwab, G. Leshkevich, D. Beletsky, N. Hawley, and A. Clites, 2010: Development of the Great Lakes Ice-circulation Model (GLIM): Application to Lake Erie in 2003–2004. *J. Great Lakes Res.*, **36**, 425–436, <https://doi.org/10.1016/j.jglr.2010.04.002>.
- Webb, E. K., G. I. Pearman, and R. Leuning, 1980: Correction of flux measurements for density effects due to heat and water vapour transfer. *Quart. J. Roy. Meteor. Soc.*, **106**, 85–100, <https://doi.org/10.1002/qj.49710644707>.
- Weisman, M. L., and Coauthors, 2015: The Mesoscale Predictability Experiment (MPEX). *Bull. Amer. Meteor. Soc.*, **96**, 2127–2149, <https://doi.org/10.1175/BAMS-D-13-00281.1>.
- Wright, D. M., D. J. Posselt, and A. L. Steiner, 2013: Sensitivity of lake-effect snowfall to lake ice cover and temperature in the Great Lakes region. *Mon. Wea. Rev.*, **141**, 670–689, <https://doi.org/10.1175/MWR-D-12-00038.1>.
- Xue, P., J. S. Pal, X. Ye, J. D. Lenters, C. Huang, and P. Y. Chu, 2016: Improving the simulation of large lakes in regional climate modeling: Two-way lake-atmosphere coupling with a 3D hydrodynamic model of the Great Lakes. *J. Climate*, **30**, 1605–1627, <https://doi.org/10.1175/JCLI-D-16-0225.1>.
- Zhao, Q., and F. H. Carr, 1997: A prognostic cloud scheme for operational NWP models. *Mon. Wea. Rev.*, **125**, 1931–1953, [https://doi.org/10.1175/1520-0493\(1997\)125<1931:APCSFO>2.0.CO;2](https://doi.org/10.1175/1520-0493(1997)125<1931:APCSFO>2.0.CO;2).